Generalized DFT-s-OFDM Waveforms Without Cyclic Prefix

Berardinelli, Gilberto

Published in:
IEEE Access

DOI (link to publication from Publisher):
10.1109/ACCESS.2017.2781122

Publication date:
2018

Document Version
Publisher's PDF, also known as Version of record

IEEE Access
Multidisciplinary | Rapid Review | Open Access Journal

Received October 31, 2017, accepted December 1, 2017, date of publication December 7, 2017,
date of current version February 28, 2018.

Digital Object Identifier 10.1109/ACCESS.2017.2781122

Generalized DFT-s-OFDM Waveforms Without Cyclic Prefix

GILBERTO BERARDINELLI, **(Member, IEEE)**
Department of Electronic Systems, Aalborg University, 9220 Aalborg, Denmark
e-mail: gb@es.aau.dk

ABSTRACT This paper deals with generalized discrete Fourier transform—spread—orthogonal frequency division multiplexing (G-DFT-s-OFDM) waveforms, which replace the cyclic prefix of traditional OFDM/DFT-s-OFDM with an internal guard period. Such waveforms feature significant benefits in terms of flexibility, spectral containment, and low peak-to-average power ratio. Aspects related to reference sequence design and mapping for channel estimation are thoroughly addressed, and a new estimator for the specific zero-tail DFT-s-OFDM case is proposed. Furthermore, we address the opportunity of exploiting the internal guard period at each symbol for frequent channel state information updates, thus enabling the possibility of tracking rapidly varying propagation conditions.

INDEX TERMS OFDM, DFT-s-OFDM, CP, ZT DFT-s-OFDM, UW DFT-s-OFDM.

I. INTRODUCTION

In Orthogonal Frequency Division Multiplexing (OFDM) -based systems, the usage of a Cyclic Prefix (CP) allows to convert the linear convolution with the fading channel to a circular convolution, leading to a simple one-tap frequency domain equalization at the receiver [1]. Thanks to its capability of efficiently counteracting the multipath, CP-OFDM has been accepted as basic waveform for several radio access technologies, including Long Term Evolution (LTE) [2] and IEEE 802.11 [3]. It has recently been agreed that also 5th Generation (5G) new radio (NR) will be adopting CP-OFDM, at least for enhanced mobile broadband (eMBB) and ultra reliable low latency communication (URLLC) services at below 40 GHz carriers [4]. The Discrete Fourier Transform -spread- OFDM (DFT-s-OFDM) waveform is meant at reducing the peak-to-average power ratio (PAPR) of OFDM by emulating a single carrier transmission, and can be obtained as a simple *add on* over OFDM [5]. Already adopted in LTE uplink, DFT-s-OFDM will also be supported by 5G NR, targeting uplink coverage-limited cases [4].

However, CP-based waveforms are known to suffer from limited flexibility and poor spectral containment. The limited flexibility is due to the necessity of predefining the CP duration as a trade-off between expected delay spread and necessity to fit a certain frame numerology. For instance, the two frame structures defined for LTE are linked to the two different CP options of $\sim 4.71\mu$s and $\sim 16.67\mu$s, the latter mainly adopted for Multimedia Broadcast Multicast Service (MBMS) [2]. The poor spectral containment is due to the abrupt transition between adjacent time symbols, and is known to significantly affect the performance of asynchronous users allocated to neighbor portions of the bandwidth. Moreover, 5G is advocating the usage of different subcarrier spacings and Time Transmission Intervals (TTIs) in neighbor frequencies as a solution to accommodate services with different latency targets in the same frame [6], [7]; such scenarios also leads to an increased sensitivity to spectral leakage.

In the recent literature, DFT-s-OFDM waveforms without CP have been proposed with the aim of circumventing the aforementioned demerits [8], while avoiding dramatic complexity increase of approaches such as Filter Bank Multicarrier (FBMC) [9] or Generalized Frequency Division Multiplexing (GFDM) [10]. Our initial work on Zero-Tail DFT-s-OFDM (ZT DFT-s-OFDM) [11] has paved the way to a set of solutions which overcome the limited flexibility of CP-based waveform and have the further potential of reducing the out-of-band emission. To mention a few, Unique Word DFT-s-OFDM (UW DFT-s-OFDM) [12] and Guard Interval DFT-s-OFDM (GI DFT-s-OFDM) [13] have been drawing significant attention in the research community. The main principle of such solutions is to replace the CP with an internal guard period whose length can be tuned accordingly to the estimated delay spread of the channel. In the case of

ZT DFT-s-OFDM, the internal guard period is composed of low power samples, while for the other schemes a predefined known word is inserted at the tail of the signal. This overcomes the poor scalability of CP-based waveforms since the radio numerology can be designed independently from the characteristics where the radio system is intended to operate; the length of the guard period can be dynamically tuned to match the instantaneous estimated delay spread without impacting the symbol duration. Moreover, in case the same sequences are used at tail and head of each signal, the transition between adjacent symbols is smoothened with benefits in terms of spectral containment.

The signal properties of DFT-s-OFDM waveforms without CP have been extensively studied with particular emphasis on their out-of-band emission performance. Further enhancements on spectral containment based on the insertion of a redundant vector have been presented in [12]. However, the recent literature tends to disregard the concerns related to practical applicability of these waveforms in a real system. For instance, channel estimation has not been yet been extensively treated. Accommodating reference sequences for channel estimation in DFT-s-OFDM waveforms without CP is indeed not straightforward, and an improper design can affect the estimation quality leading to poor link performance. Widely used sequences such as Zadoff-Chu (ZC) [14] benefit from attractive properties in terms of autocorrelation and flat frequency response, which can be negatively affected by the necessity of multiplexing them with a predefined word within the IFFT window. Further, the opportunities for exploiting the tail of the signal for further purposes than enhanced flexibility and improved spectral containment, have not been thoroughly assessed.

In this article, we present an unified framework for DFT-s-OFDM waveforms without CP and discuss challenges and opportunities, with particular emphasis on reference sequence design and mapping. We refer to such framework as Generalized DFT-s-OFDM (G-DFT-s-OFDM), which includes both cases of nearly-zero power tail (ZT DFT-s-OFDM) and known sequence tail (UW DFT-s-OFDM). Through the article, we distinguish between ZT DFT-s-OFDM and UW DFT-s-OFDM when discussing specific features and challenges, and simply refer to G-DFT-s-OFDM for aspects which are common to both waveforms. We first describe signal generation and main properties and benefits, including a mathematical analysis of the energy leakage of the data on the tail of the signal since this has an impact on the required overhead and on the spectral containment. We present approaches for harmlessly accommodating reference sequences without significantly compromising the G-DFT-s-OFDM properties. Further, opportunities in terms of frequent updates of the channel estimate, for e.g. tracking fast time-varying channels, which are not possible in traditional DFT-s-OFDM with CP will be highlighted.

The article is structured as follows. The design of the G-DFT-s-OFDM signal along with a description of its tail energy leakage characteristic is presented in Section II.

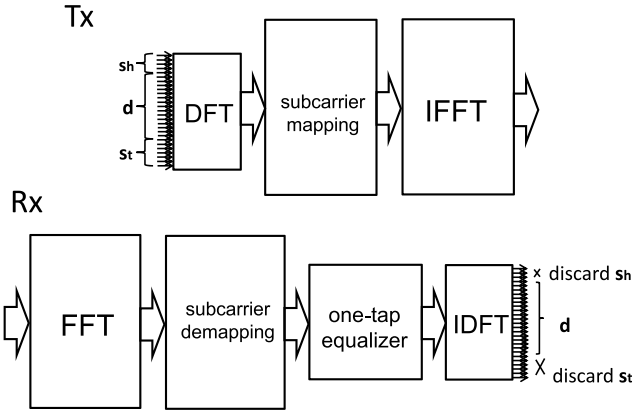

FIGURE 1. Structure of G-DFT-s-OFDM baseband transceiver.

The main benefits of the waveforms are described in Section III. Section IV discusses the problem of achieving reliable channel estimation, emphasizing specific concerns for the ZT DFT-s-OFDM case. Section V describes how G-DFT-s-OFDM can be used to track fast channel variations. A performance analysis is carried out in Section VI. Finally, Section VII concludes the article.

II. SIGNAL GENERATION AND DETECTION

The generation of a G-DFT-s-OFDM signal is presented in this section, along with a description of its basic properties. The baseband transceiver structure is displayed in Figure 1. Let us consider a generic data vector $\mathbf{d}$ having length $\tilde{N}$, which is mapped over the following column vector:

$$\mathbf{q} = [\mathbf{s}_h \; \mathbf{d} \; \mathbf{s}_t]^T \tag{1}$$

where $(\cdot)^T$ denotes the transpose operator, and $\mathbf{s}_h$ and $\mathbf{s}_t$ are known head and tail sequences having length N_h and N_t, respectively. A possible design for the sequences $\mathbf{s}_h$ and $\mathbf{s}_t$ will be discussed in Section IV. The $\mathbf{q}$ vector having length $N = \tilde{N} + N_h + N_t$ is fed to a DFT block, whose output is then mapped over the frequency subcarriers and IFFT-processed. The resultant $N_{FFT} \times 1$ time signal vector $\mathbf{y}$ can be then expressed as

$$\mathbf{y} = \mathbf{F}_{N_{FFT}}^{-1} \mathbf{M} \mathbf{F}_N \mathbf{q}, \tag{2}$$

where $\mathbf{F}_P$ denotes the $P \times P$ FFT matrix, i.e.

$$\mathbf{F}_P[a, b] = \frac{1}{\sqrt{P}} e^{-\frac{j2\pi ab}{P}} \tag{3}$$

for $a = 0, \cdots, P-1$, $b = 0, \cdots, P-1$ and $\mathbf{M}$ is the $N_{FFT} \times N$ matrix which maps the data on the frequency subcarriers (subcarrier mapping matrix). A localized subcarrier mapping is here assumed [5]. Given the linearity of the involved operations, the resultant signal can also be expressed as $\mathbf{y} = \mathbf{y}_{s_h} + \mathbf{y}_d + \mathbf{y}_{s_t}$, where $\mathbf{y}_{s_h} = \mathbf{V}\left[\mathbf{s}_h \; \mathbf{0}_{(N-N_h)}\right]^T$, $\mathbf{y}_d = \mathbf{V}\left[\mathbf{0}_{N_h} \; \mathbf{d} \; \mathbf{0}_{N_t}\right]^T$ and $\mathbf{y}_{s_t} = \mathbf{V}\left[\mathbf{0}_{(N-N_h)} \; \mathbf{s}_t\right]^T$, with $\mathbf{V} = \mathbf{F}_{N_{FFT}}^{-1} \mathbf{M} \mathbf{F}_N$ and $\mathbf{0}_x$ denoting a vector of zeros having length x. It is known that a cascade of DFT, subcarrier

mapping and IFFT blocks represented by the $\mathbf{V}$ matrix corresponds to a Dirichlet filter which localizes the significant part of the energy of each input data symbol in a specific output sample [15]. It is possible then to identify the portions $\tilde{\mathbf{y}}_{s_h}$,$\tilde{\mathbf{y}}_{s_d}$, $\tilde{\mathbf{y}}_{s_t}$ of the output vectors having length N_{s_h}, N_d, N_{s_t}, respectively, such that the following relationships hold:

$$\sum_{n=0}^{N_{s_t}-1} \left|\tilde{\mathbf{y}}_{s_t}[n]\right|^2 \approx \sum_{n=0}^{N_{FFT}-1} \left|\mathbf{y}_{s_t}[n]\right|^2, \tag{4}$$

$$\sum_{n=N_{s_t}}^{N_{s_t}+N_d-1} \left|\tilde{\mathbf{y}}_{d}[n]\right|^2 \approx \sum_{n=0}^{N_{FFT}-1} \left|\mathbf{y}_{d}[n]\right|^2, \tag{5}$$

$$\sum_{n=N_{s_t}+N_d}^{N_{FFT}-1} \left|\tilde{\mathbf{y}}_{s_h}[n]\right|^2 \approx \sum_{n=0}^{N_{FFT}-1} \left|\mathbf{y}_{s_h}[n]\right|^2. \tag{6}$$

In other terms, each of the vectors contributing to the output signal features a significant energy only over a portion of the samples. The three signal components are shown in Figure 2, which also illustrates how each component suffers from the leakage of the other two components when combined. Note that the signal $\mathbf{y}_d$ corresponds to the case in which the two known sequences $\mathbf{s}_h$ and $\mathbf{s}_t$ in Eq.(1) are zero-vectors; this option leads to the ZT DFT-s-OFDM waveform [11]. The length of the significant energy parts of the output signal is given by $N_{s_h} = \left\lfloor \frac{N_h N_{FFT}}{N} \right\rfloor$, $N_d = \left\lfloor \frac{\tilde{N} N_{FFT}}{N} \right\rfloor$ and $N_{s_t} = \left\lfloor \frac{N_t N_{FFT}}{N} \right\rfloor$, respectively, where $\lfloor x \rfloor$ denotes the nearest integer number higher than x [11].

Though the sequences $\mathbf{s}_h$ and $\mathbf{s}_t$ can be set to be identical at consecutive symbols in a frame and lead to identical $\mathbf{y}_{s_h}$ and $\mathbf{y}_{s_t}$ sequences, in practice the head and the tail of the signal are only *quasi*-identical since they contain the energy leakage from the data vector $\mathbf{d}$, which varies at each symbol. Such leakage is the only visible term of the output signal in case of ZT DFT-s-OFDM waveform, and is significantly lower than the average signal power (e.g., 25 dB lower with the numerology shown in Figure 2) [11]. A detailed characterization of the leakage will be presented in the next subsection.

The usage of $\mathbf{y}_{s_t}$ at each data symbol is meant to generate the same intersymbol interference component that the symbol experiences at its beginning, provided its length is set to be longer than the delay spread of the wireless channel; this leads to a cyclic signal which enables the usage of efficient one tap frequency domain equalization. For the case of ZT DFT-s-OFDM, the low power tail is instead coping with the delay spread of the channel within the symbol itself. In both cases, non-cyclic intersymbol interference is therefore reduced to the energy spillover of the data part to the next symbol. $\mathbf{y}_{s_h}$ is instead only meant to avoid power regrowth of the data part in the last samples of the symbols due to the cyclicity of IFFT operation [16]; it then represents a pure overhead term. It is worth to observe that the usage of the same head and tail vectors smoothens the abrupt transitions between adjacent time symbols; this is expected to reduce the out-of-band emissions of the signals with respect to baseline

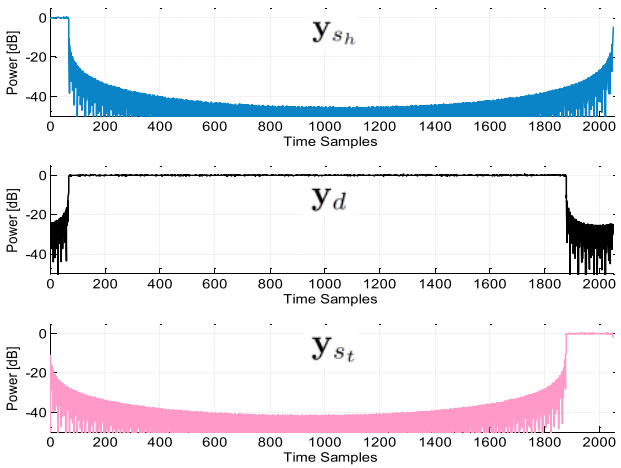

FIGURE 2. Components of a G-DFT-s-OFDM signal, assuming N=1200, N_{s_t}=144, N_{s_h}=17, N_{FFT} = 2048. The component $\mathbf{y}_d$ represents a ZT DFT-s-OFDM signal.

OFDM/DFT-s-OFDM. Further, similarly to traditional DFT-s-OFDM, the G-DFT-s-OFDM waveform benefits from low power amplitude fluctuations since it emulates a single carrier transmission. Both aspects will be clarified in the performance evaluation section.

The generated signal vector is then transmitted over the air at a sample rate $S = N_{FFT}\Delta f$, where Δf denotes the subcarrier spacing. In case of ideal unitary channel response and absence of Gaussian noise, the transmit vector $\mathbf{q}$ can be retrieved as:

$$\mathbf{q} = \mathbf{F}_N^{-1}\mathbf{M}^{-1}\mathbf{F}_{N_{FFT}}\mathbf{r} \tag{7}$$

where $\mathbf{r} = \mathbf{y}$ denotes the received signal, and the original data vector is obtained by discarding the head and tail sequences, i.e.

$$\mathbf{d} = \mathbf{q}\,[N_h : (N - N_t - 1)]. \tag{8}$$

With transmission over a fading channel, frequency domain equalization can be applied as in traditional OFDM and DFT-s-OFDM systems.

Since the operations in Eq.(1) and Eq.(8) are trivial, the complexity of the G-DFT-s-OFDM transceiver is the same as the traditional uplink LTE transceiver [17]. Moreover, the extension to Multiple-Input-Multiple-Output (MIMO) antenna transmission schemes is as straightforward as in any OFDM/DFT-s-OFDM scheme thanks to the subcarrier-wise processing. Unfortunately, as in traditional DFT-s-OFDM the data symbols are spread over the entire bandwidth, and this prevents the usage of frequency selective scheduling or link adaptation [18]. However, the possibility of applying frequency selective algorithms can be kept in case the DFT-spreading is applied, for instance, on a frequency resource block basis rather than on the entire bandwidth. We refer to [19] for an extensive description of such options.

A. LEAKAGE ANALYSIS

Ideally, we are pursuing signals having identical tail, which guarantees perfect cyclicity across adjacent symbols in case of transmission over time dispersive channels. However, as argued above, the tail of each signal is affected by the energy leakage from the **d** vector which varies at each symbol. An analysis of the leakage of the **d** vector on the signal tail is here provided, with the aim of quantifying its effective impact.

Let us denote with N_{s_0} the total length of the signal portion non dedicated to data, i.e. $N_{s_0} = N_{s_h} + N_{s_t}$. For the sake of simplicity, without loss of generality, we assume for the moment $N_{s_h} = 0$. Let us consider the following partition of the **V** matrix:

$$\tilde{\mathbf{V}} = \mathbf{V}\left(N_{FFT} - N_{s_t} : N_{FFT} - 1, 0 : N - N_t - 1\right). \quad (9)$$

We can then express the leakage of the data vector **d** on the signal tail as $\hat{\mathbf{y}}_d = \tilde{\mathbf{V}}\mathbf{d}$. The vector of the average power of the leakage $\hat{\mathbf{y}}_d$ is given by:

$$\mathbf{p}_{\hat{\mathbf{y}}_d} = E\left\{diag\left(\hat{\mathbf{y}}_d\hat{\mathbf{y}}_d^H\right)\right\} = E\left\{diag\left(\tilde{\mathbf{V}}\mathbf{d}\mathbf{d}^H\tilde{\mathbf{V}}^H\right)\right\}, \quad (10)$$

where $E\{\cdot\}$ denotes the expectation operation, $(\cdot)^H$ is the hermitian operator and $diag(\cdot)$ returns the diagonal of the matrix where it is applied. Since the only random term in Eq.(10) is given by the data vector **d**, it can be rewritten as follows:

$$\mathbf{p}_{\hat{\mathbf{y}}_d} = diag\left(\tilde{\mathbf{V}}E\left\{\mathbf{d}\mathbf{d}^H\right\}\tilde{\mathbf{V}}^H\right) \quad (11)$$

Traditional data symbol constellations are defined in a way that their average power is unitary, i.e. $E\left\{\mathbf{d}\mathbf{d}^H\right\} = \mathbf{I}_{N-N_t}$, where $\mathbf{I}_P$ denotes the $P \times P$ identity matrix. The elements of $\mathbf{p}_{\hat{\mathbf{y}}_d}$ can be then expressed as:

$$p_m = \left|\hat{\mathbf{y}}_d(m)\right|^2 = \sum_{k=0}^{N-N_t-1}\left|\tilde{\mathbf{V}}(m,k)\right|^2 \quad (12)$$

for $m = 0 : N_{s_t} - 1$. By exploiting the identity $sin(x) = \left(e^{jx} - e^{-jx}\right)/2j$, it can by by straightforward calculations that Eq.(12) can be expressed as the product of two independent functions:

$$p_m = \theta_1(m)\,\theta_2(m) \quad (13)$$

with

$$\theta_1(m) = sin^2\left(\frac{\pi N\left(m + N_{FFT} - N_{s_t}\right)}{N_{FFT}}\right), \quad (14)$$

$$\theta_2(m) = \frac{1}{N^2}\sum_{k=0}^{N-N_t-1} csc^2\left(\frac{\pi\left(m + N_{FFT} - N_{s_t}\right)}{N_{FFT}} - \frac{\pi k}{N}\right). \quad (15)$$

Both θ_1 and θ_2 functions are displayed in Figure 3. θ_1 represents the oscillating part of the leakage component, while θ_2 is its envelope. θ_2 is a convex function and is nearly symmetrical with respect to its minimum. The power regrowth at the last samples is due to the cyclicity of the IFFT which appears in Eq.(2). By placing a known sequence $\mathbf{s}_h$ at the beginning of the vector, the last N_{s_h} samples of θ_2 are cyclically shifted to the beginning, leading to a shape similar to the second subplot in Figure 2. $\mathbf{s}_h$ represents pure overhead and its length should be minimized. N_{s_h} can be parametrized as follows (see Figure 3(b)):

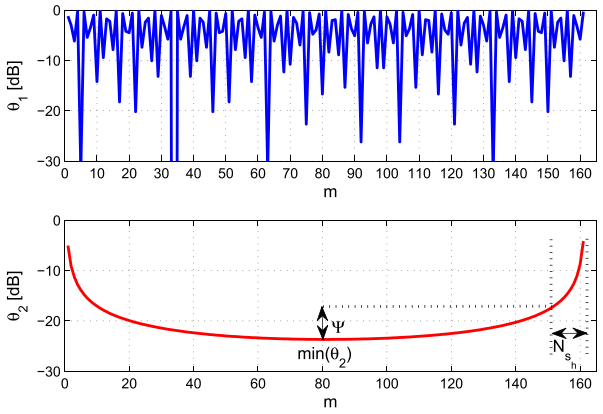

FIGURE 3. Oscillating part and envelope of the leakage, assuming N=1200, N_{FFT}=2048, N_{s_0}=161.

$$N_{s_h} = N_{s_0} - \theta_2^{-1}\left(min\left(\theta_2\right) + \Psi\right) \quad (16)$$

where Ψ represents the acceptable offset of power regrowth with respect to the minimum of the θ_2 function, and f^{-1} stands here for the inverse of the function f. Figure 4 shows the overhead of N_h as a function of the total number of data subcarriers, assuming N_{FFT}=2048, for different values of Ψ. Obviously, N_h decreases with the increase of Ψ; a shorter known head is needed in case larger power regrowth can be tolerated. It is also obvious from Eq.(15), that the minimum value of the energy leakage decreases as the number of subcarriers N increases; this translates to the observation that both link performance and spectral contaiment improve for large bandwidth allocation since the effect of the leakage in the signal tail will be diminished. This is also shown in [11]. Note that the slope of the curves decreases with Ψ; this means, a smaller relative overhead is needed for large bandwidth allocations to achieve a certain power suppression. The impact of different power suppression levels on the spectral containment will be shown next.

III. GENERAL BENEFITS

This section presents a qualitative overview of the main benefits of G-DFT-s-OFDM with respect to CP-based waveforms.

A. UNIFIED NUMEROLOGY AMONG DIFFERENT CELLS

The G-DFT-s-OFDM waveform copes with the time dispersion characteristics of the radio channel without a CP, and therefore avoiding its inefficiencies. In current radio technologies the CP is predefined in the system numerology, leading to potential spectral efficiency losses in case of propagation over channels with shorter delay spread, or to a Block Error Rate (BLER) increase in case its length is insufficient.

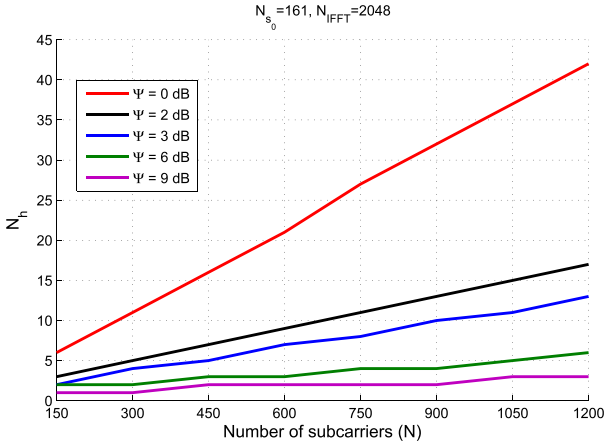

FIGURE 4. Overhead of the known head sequence.

Further, the insertion of CP leads to a poor coexistence among systems operating with different settings. A larger time dispersion requires indeed a longer CP, but the duration of the IFFT output needs to remain the same to maintain the system numerology. This leads to different symbol durations as well as to a different number of symbols per frame. Cells adopting different CP durations generate then mutual asynchronous interference even when aligned at frame level. Computationally feasible interference-aware receivers such as Interference Rejection Combining (IRC) [20] and Successive Interference Cancellation (SIC) [21] are able to efficiently suppress synchronous interfering streams but fail their task in case of asynchronous interference. In G-DFT-s-OFDM, the length of the tail, which is meant to cope with the time dispersion of the channel, can be set accordingly to the experienced delay spread and is absorbed within the symbol. In this way, G-DFT-s-OFDM allows decoupling the radio numerology from the channel characteristics, simplifying the system design and enabling the possibility of synchronizing radio links regardless of the cell size and experienced propagation conditions.

Note that, differently from traditional OFDM/DFT-s-OFDM, the lack of CP allows G-DFT-s-OFDM to scale the number of symbols per frame proportionally to the reduction/increase of the symbol duration (and therefore to the increase/reduction of the subcarrier spacing). In other words, given a predefined frame duration, by reducing of a factor X the symbol time, an X-times higher number of symbols fits perfectly the same frame. This eases the scalability to different subcarrier spacings as advocated in [6] and confirmed in recent 3GPP agreements [4] as a solution to cope with diverse 5G services within the same frequency band.

B. IMPROVED COEXISTENCE AMONG DEVICES TRANSMITTING OVER ADJACENT CHANNELS

Besides co-channel interference, the power leakage over adjacent frequency chunks can significantly affect the cell throughput performance. By using an OFDM/DFT-s-OFDM modulation, the signals transmitted over different frequency resources are orthogonal only in case the transmitters are time-synchronized [19]. However, time misalignment would affect negatively frequency multiplexed signals due to the poor spectral containment of OFDM. The application of a raised cosine filter can be used for shaping the OFDM spectrum [1]; nevertheless, this comes at the expense of a throughput loss and/or BLER increase. The occurrence of asynchronous transmissions in neighbor bands is expected to be a recurrent phenomenon in 5G. For instance, mMTC sporadic transmission may only be coarsely synchronized to the network. Further, in 5G NR users operating in adjacent frequency chunks may be using different symbol durations, therefore misaligning their transmissions. G-DFT-s-OFDM features the advantage of an improved spectral containment with respect to CP-based transmission, while avoiding signal distortion of e.g. raised cosine windowing. The improved spectral containment translates to a diminished mutual interference among users operating over neighbor frequency chunks in case of time misaligned transmissions. Note however that, in traditional OFDM/DFT-s-OFDM, the CP provides a tear of protection towards time misalignment. In G-DFT-s-OFDM the non-ideality of the head/tail of the signal leads to a residual interference power which is independent from the specific time offset. Such residual interference is however significantly lower than the one experienced by OFDM/DFT-s-OFDM for larger offsets than the CP duration. We refer to our previous contribution [16] for a detailed analysis of residual interference for time misaligned users.

C. SUPPORT OF AGILE LINK DIRECTION SWITCHING

Time Division Duplex (TDD) mode is considered a valid solution for coping with high bursty traffic, and has significant potential especially in small cells due to the low flow aggregation level [22]. A proper usage of TDD mode assumes the system can support the possibility of changing the transmission direction rather often [23], and every transition requires the presence of a guard period (GP) to accommodate the on/off power transient. Similarly to the CP in OFDM, the duration of such GP is typically hard-coded in the system numerology, and is conceived as a distinct overhead term in the frame. For instance, in LTE-TDD the GP is located in a special subframe and occupies at least the duration of an entire OFDM symbol [24]. While the LTE specifications consider an on/off power transient of 20 μs [17], in a future 5G system such transient is envisioned to be significantly shorter due to the lower transmit power and the expected evolution of the analog switches, e.g. lower than 60 ns [25].

By using ZT DFT-s-OFDM, the GP can be included in the last part of the time symbol rather than being an additional time gap. Further, its length can also be tuned according to the estimated duration of the on/off power transient. Note that the insertion of the GP in the bottom part of the time symbol subsumes the last samples of the low power tail to be cut-off. In principle, this may impact the orthogonaliy of the subcarriers of the received signals. However, such

degradation has been shown to be minimal given the low power magnitude of the samples [16]. Observe that the same principle of embedding the GP in the symbol can be used for providing a dead time for ramping down and ramping up radio beams at mm-wave communications [26]. Such dead time can be also tuned according to the hardware capabilities rather than being set as a predefined time interval.

IV. CHANNEL ESTIMATION IN G-DFT-s-OFDM

As mentioned in the introduction, the recent literature on DFT-s-OFDM waveforms without CP has a major focus on their spectral containment properties and coexistence of users transmitting over neighbor bands, disregarding concerns related to their practical usage such as the possibility of acquiring accurate channel state information. Solution for mapping reference sequences (RSs) and acquiring channel estimation in G-DFT-s-OFDM are described in this section, with a distinction for the cases of ZT DFT-s-OFDM and UW DFT-s-OFDM.

It is known that channel estimation exploits advantageous properties of a certain set of complex sequences. For the rest of the article, we will consider Zadoff-Chu (ZC) sequences as RSs for G-DFT-s-OFDM, though the described solution can be generalized to other families of sequences. ZC sequences are a family of complex sequences featuring zero autocorrelation and constant cross-correlation limited to $\sqrt{L}$, where L is the length of the sequence. Further, ZC sequences have constant amplitude over both time and frequency domain. In case the length L of the ZC sequence is a prime number, the set of sequences fulfilling the mentioned properties has cardinality equal to $L-1$. The n^{th} entry of the k^{th} sequence, with $k \in \{1, \ldots, L-1\}$, is given by

$$c_k(n) = e^{\frac{j2k\pi}{L}\left(n+n\frac{n+1}{2}\right)}, \tag{17}$$

for $n = 0, \cdots, L-1$. ZC sequences have been widely used in LTE uplink for the Demodulation Reference Symbols (DMRSs) and the Sounding Reference Signals (SRSs) [2].

A. UW DFT-s-OFDM CASE

In UW DFT-s-OFDM, mapping RSs for channel estimation requires specific measures for preserving the cyclicity of the received signal. Let us consider a frame composed of Q UW DFT-s-OFDM symbols, where $Q-1$ symbols are dedicated to data, and the remaining symbol is dedicated to the RS.

The RS symbol can be generated by replacing the vector $\mathbf{q}$ in Eq.(1) with the reference vector $\mathbf{c}_t$ of length N, i.e. $\mathbf{q} = \mathbf{c}_t$. We assume that such vector corresponds to the discrete time domain version of a frequency generated reference sequence $\mathbf{c}$, i.e.

$$\mathbf{c}_t = \mathbf{F}_N^H \mathbf{c}^T. \tag{18}$$

A cyclic shift δ can be eventually applied, leading to the sequence $\mathbf{c}_t^\delta = \mathbf{c}_{\delta mod\, N}$. Such sequence is then mapped over the used subcarriers and IFFT processed as every data symbol. The resultant time domain vector $\mathbf{s}$ reads

$$\mathbf{s} = \mathbf{F}_{N_{FFT}}^H \mathbf{M} \mathbf{c}_t^\delta, \tag{19}$$

The generated signal is transmitted over the air at a sample rate $S = N_{FFT}\,\Delta f$. The received signal vector is given by

$$\mathbf{r} = \mathbf{s} \otimes \mathbf{h} + \mathbf{w}, \tag{20}$$

where $\otimes$ is the convolution operator, $\mathbf{w}$ is the additive white gaussian noise vector, and $\mathbf{h}$ is the impulse response vector of the fading channel having length equal to $n = \tau_{ds}/S$, with τ_{ds} denoting the instantaneous delay spread of the channel. The reverse operations are then taken. The processed received signal is given by

$$\tilde{\mathbf{r}} = \mathbf{F}_N^{-1} \mathbf{M}^T \mathbf{F}_{N_{FFT}} \check{\mathbf{r}}^T. \tag{21}$$

where $\check{\mathbf{r}} = \mathbf{r}\,(1 : N_{IFFT})$. An estimate of the channel impulse response is then obtained by correlating the $\tilde{\mathbf{r}}$ signal against the transmit sequence, i.e.

$$\hat{\mathbf{h}}_0 = \mathbf{R}_{c_t \tilde{r}}. \tag{22}$$

where $\mathbf{R}_{xy}$ denotes the cyclic correlation of two sequences x and y having equal length. Note that, thanks to the zero-autocorrelation properties of the ZC sequences, $\hat{\mathbf{h}}_0$ has useful energy only over a number of samples $n' = n \cdot N/N_{FFT}$, while the rest of the samples only introduces further noise or interference. It is worth observing that Eq.(22) omits the δ index since it is possible with an unique correlator to estimate multiple channel responses [14]. For a specific δ shift, an estimate of the impulse response can be obtained as follows:

$$\hat{\mathbf{h}} = \left[\hat{\mathbf{h}}_0\left(\delta : n' + \delta - 1\right) \quad \mathbf{0}_{N-n'}\right]. \tag{23}$$

In case the low power tail is longer than the delay spread of the channel, i.e. $N_{s_t} > n$, it can be easily shown that $\hat{\mathbf{h}} \approx \mathbf{F}_N^H \mathbf{M}^T \mathbf{F}_{N_{FFT}} \bar{\mathbf{h}}^T + \bar{\mathbf{w}}$, where $\bar{\mathbf{h}}$ is the zero-padded version of $\mathbf{h}$ having length N_{FFT}, and $\bar{\mathbf{w}} = \mathbf{F}_N^H \mathbf{M}^T \mathbf{F}_{N_{FFT}} \mathbf{w}^T$. In a practical implementation, several advanced estimators such as Wiener filter can also be used for reducing the impact of the residual noise power [27]. The estimated vector can be then converted to the frequency domain vector $\hat{\mathbf{H}} = \mathbf{F}_N \hat{\mathbf{h}}$ to be used for one-tap equalization. An alternative receiver implementation where the correlation is converted to a frequency domain one-tap multiplication is possible for the sake of complexity reduction [28].

Note that an implicit assumption for retrieving a correct channel estimate, is that the symbol where the RS is mapped experiences a cyclic fading. In order to enable this, we propose here to generate the known sequences $\mathbf{s}_h$ and $\mathbf{s}_t$ at each data symbol as a copy of the first and last samples of the $\mathbf{c}_t$ vector, i.e.

$$\mathbf{s}_h = \mathbf{c}_t\,(0 : N_h - 1), \tag{24}$$

$$\mathbf{s}_t = \mathbf{c}_t\,(N - N_t : N - 1). \tag{25}$$

The principle is shown in Figure 5, where the cases of different symbol durations are also considered. This approach exploits the degree of freedom offered by the presence of

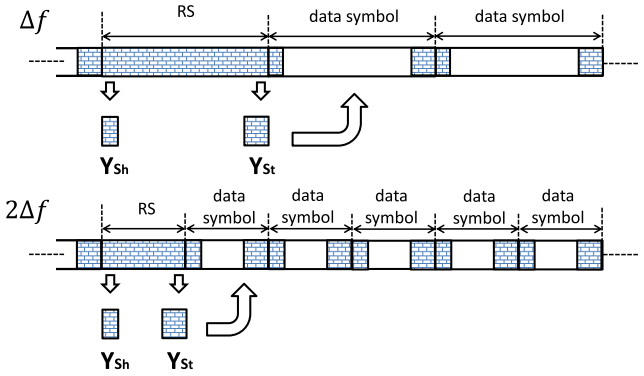

FIGURE 5. Proposed reference sequence mapping for UW DFT-s-OFDM.

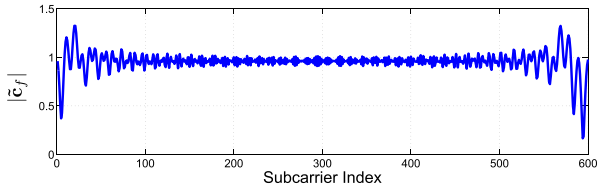

FIGURE 6. Non-flat frequency response of the zero-padded reference sequence, assuming N=600, N_h=4, N_t=42.

the $\mathbf{s}_t$ and $\mathbf{s}_h$ vectors to harmlessly accommodate the reference sequence in the radio frame. The cyclicity property is nearly maintained; the only degradation term with respect to traditional CP waveforms is again due to the energy leakage of the data samples in the tail. Further, this solution allows exploiting the tail of the signal for frequently updating the channel estimate, as will be elaborated in the next section.

B. ZT DFT-s-OFDM CASE

While the UW DFT-s-OFDM nature offers a rather simple solution for allocating the RSs in a time symbol, channel estimation for ZT DFT-s-OFDM is not a straightforward task due to the constraint of generating a low power head and tail also for the RS symbol. In this case, the frequency domain RS $\mathbf{c}$ must be generated having a length equal to $\tilde{N} = N - N_t - N_h$. The time domain reference sequence reads then

$$\mathbf{c}_t = \mathbf{F}_{\tilde{N}}^H \mathbf{c}^T, \tag{26}$$

A cyclic shift δ can be eventually applied, leading to the sequence $\mathbf{c}_t^\delta = \mathbf{c}_{\delta mod\ \tilde{N}}$. According to the ZT DFT-s-OFDM processing, such sequence is zero-padded as follows:

$$\tilde{\mathbf{c}}_t^\delta = \left[\mathbf{0}_{N_h} \quad \left(\mathbf{c}_t^\delta\right)^T \quad \mathbf{0}_{N_t}\right]^T, \tag{27}$$

Such zero-insertion can affect other properties of the base sequence $\mathbf{c}_t$. For instance, in case the starting $\mathbf{c}_t$ sequence is a ZC sequence, the zero-vector insertion also leads to a degradation of the frequency domain response $\tilde{\mathbf{c}}_f$ of $\tilde{\mathbf{c}}_t$, as shown in Figure 6. This in turn affects the autocorrelation property of the sequence, leading to a poor quality channel estimation.

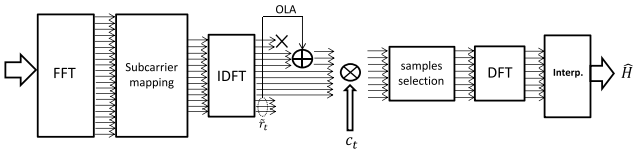

FIGURE 7. Proposed channel estimator for ZT DFT-s-OFDM.

Moreover, since the eventual cyclic shift needs to be applied before zero-padding, sequences obtained with different cyclic shifts of the same base sequence translate to sequences that are not cyclic anymore. In other words, given the shift values δ_1 and δ_2, with $\delta_1 \neq \delta_2$, the sequences $\mathbf{c}_t^{\delta_1}$ and $\mathbf{c}_t^{\delta_2}$ are cyclic, but the same does not hold for $\tilde{\mathbf{c}}_t^{\delta_1}$ and $\tilde{\mathbf{c}}_t^{\delta_2}$. It is therefore not possible to correctly retrieve multiple channel responses with an unique correlator. The received signal should be correlated against the sequence obtained from the specific δ shift applied at the transmitter. This increases the receiver complexity. In our previous contribution [29], we have proposed a technique for distorting the original $\mathbf{c}_t$ sequence such that its zero-padded version $\tilde{\mathbf{c}}_t$ mantains a flat frequency response. This allows to preserve the autocorrelation properties at the receiver, improving the quality of the channel estimation. Nonetheless, cyclic shifted version of the same base sequence still leads to non-cyclic distorted versions of the over-the-air signal. Further, the non-cyclic distorted versions also generate mutual interference when transmitted simultaneously, causing significant cross-correlation.

1) PROPOSED CHANNEL ESTIMATOR

We present here a channel estimator for ZT DFT-s-OFDM which aims at overcoming the aforementioned drawbacks [30]. The principle of the proposed channel estimator is to correlate the received signal against the original reference sequence rather than its zero-padded version, provided specific arrangements to restore cyclicity are taken. The structure of the estimator is shown in Figure 7. The received signal undergoes the traditional operations of FFT, subcarrier demapping and IDFT as in Eq.(21). The resultant N-length signal $\tilde{\mathbf{r}}$ at this stage can be seen as a downsampled version of the received signal $\mathbf{r}$ with length N_{FFT}. The vector $\tilde{\mathbf{r}}_t$ which represents the last N_t samples of $\tilde{\mathbf{r}}$, is expected to collect the energy leakage due to the delay spread of the wireless channel over the low-power tail of the transmit signal. Such vector is added to the first useful samples of $\tilde{\mathbf{r}}$, leading to the following $\tilde{N}$-length vector:

$$\tilde{\mathbf{r}}' = \tilde{\mathbf{r}}\,[N_h : N - N_t - 1] + \left[\tilde{\mathbf{r}}_t\ \mathbf{0}_{\tilde{N}-N_t}\right]. \tag{28}$$

Eq.(28) is meant at emulating a cyclic signal over the useful $\tilde{N}$ samples. This operation is known in signal processing as overlapp-and-add (OLA) [31] and shown in Figure 8; it allows transforming the linear convolution with the fading channel with a cyclic convolution and has been used, for instance, for the detection of Zero-Padded OFDM signals [32]. With respect to traditional cyclicity as introduced

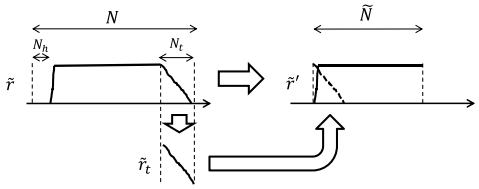

FIGURE 8. Usage of the OLA principle for emulating a cyclic fading.

by CP, OLA slightly colors the noise term [33]. The signal $\tilde{\mathbf{r}}'$ can be then correlated against the $\hat{N}$-length sequence $\mathbf{c}_t$ rather than the zero-padded sequence $\tilde{\mathbf{c}}_t^{\delta}$ to obtain an estimate of the channel impulse response, i.e.

$$\hat{\tilde{\mathbf{h}}}_{\mathbf{0}} = \mathbf{R}_{c_t \tilde{r}'}. \tag{29}$$

The first benefit of this approach, is the possibility of entirely exploiting the benefits of the original reference sequence, namely its flat frequency response and its zero-autocorrelation. For a specific δ shift, an estimate of the impulse response can be obtained as follows:

$$\hat{\mathbf{h}}_{\mathbf{0}} = \left[\hat{\tilde{\mathbf{h}}}_0 \left(\delta : \delta + n''\right) \ \mathbf{0}_{\tilde{N}-n''}\right], \tag{30}$$

where $n'' = n \cdot \tilde{N}/N_{FFT}$. The channel frequency response can be then calculated as $\hat{\mathbf{H}}_0 = \mathbf{F}_{\tilde{N}} \mathbf{h}_0$. Since $\hat{\mathbf{H}}_0$ spans $\tilde{N}$ samples, it has to be interpolated to a length N in order to get the frequency response $\hat{\mathbf{H}}$ over the used subcarriers. The obvious penalty of this approach is a loss of frequency resolution in the channel estimate of a factor $N/\tilde{N}$, which however has a minor impact for realistic channel profiles and zero-tail lengths.

V. TRACKING FAST CHANNEL VARIATIONS

In the previous section, we have presented solutions for accommodating reference sequences and estimating the channel responses for the specific cases of ZT DFT-s-OFDM and UW DFT-s-OFDM waveforms. While for ZT DFT-s-OFDM the low power tail is meant to absorb the energy dispersion of the fading channel, for UW DFT-s-OFDM the tail of the signal is meant at preserving cyclicity and can be discarded after equalization and IDFT operation. Nonetheless, such tail can be also used to estimate the frequency offset or to deal with high speed channels [34].

In this section, we describe a receiver architecture which exploits the tail of each UW DFT-s-OFDM symbol for tracking fast channel variations, with the aim of emphasizing further benefits of such waveform. As mentioned above, this is not possible with ZT DFT-s-OFDM given the nearly zero-power tail. Our receiver structure is depicted in Figure 9. The received signal is obtained from the convolution of the transmit signal with the channel impulse response $\mathbf{h}_k$ having length equal to $n = \tau_{ds}/S$, where the index k refers to the k^{th} symbol. For the sake of simplicity, we assume that the RS is mapped over the first UW DFT-s-OFDM symbol in the frame, as also shown in Figure 5.

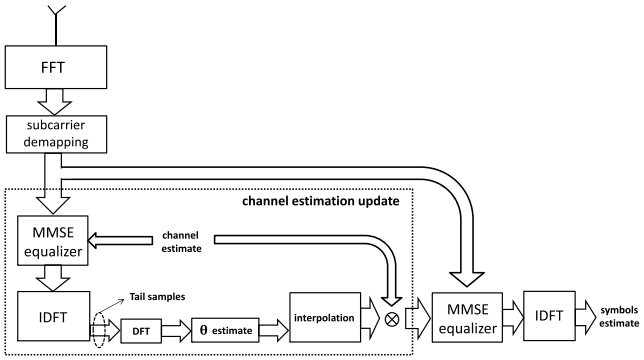

FIGURE 9. Proposed receiver architecture for tracking fast channel variations for UW DFT-s-OFDM.

With the assumption that the channel impulse response remains approximately constant within the symbol duration, and that the sequence $\mathbf{y}_{s_t}$ is longer than n, the received symbol after FFT and subcarrier demapping can be expressed as

$$\mathbf{R}_k = \mathbf{M}^T \mathbf{F}_{N_{FFT}} \mathbf{r}_k \approx \mathbf{H}_k \mathbf{Y}_k + \mathbf{W}_k, \tag{31}$$

where $\mathbf{r}_k$ is the vector collecting the received samples corresponding to the k^{th} transmit symbol $\mathbf{y}_k$, $\mathbf{Y}_k$ denotes the frequency response of $\mathbf{y}_k$ in the used subcarriers, $\mathbf{H}_k$ is the $N \times N$ diagonal matrix of the channel frequency response and $\mathbf{W}_k$ is the additive white gaussian noise vector. Eq.(31) also assumes that the residual non-cyclic inter-symbol interference due to the usage of a non-ideal $\mathbf{y}_{s_t}$ at each symbol is negligible. By assuming that an estimate of the channel frequency response $\hat{\mathbf{H}}_1$ is calculated upon reception of the RS symbol, the input data vector is estimated as

$$\hat{\mathbf{q}}_k = \mathbf{F}_N^{-1} \mathbf{P} \mathbf{R}_k, \tag{32}$$

where $\mathbf{P}$ is the equalization matrix. Minimum Mean Square Error (MMSE) equalizers are typically used with DFT-s-OFDM waveforms [35]. In this case, the equalization matrix reads

$$\mathbf{P} = \hat{\mathbf{H}}_1^H \left(\hat{\mathbf{H}}_1 \hat{\mathbf{H}}_1^H + \mathbf{\Sigma}_W\right)^{-1}, \tag{33}$$

where $\mathbf{\Sigma}_W = E\left(\mathbf{W}_k \mathbf{W}_k^H\right)$, with $(\cdot)^H$ denoting the hermitian operator. Equalization across the frame is then performed assuming the channel estimated at the first symbol. Note that $\hat{\mathbf{q}}_k$ also contains an estimate of the known tail at the k^{th} symbol $\hat{\mathbf{s}}_{t,k}$.

Let us express the channel response at the k^{th} symbol as follows:

$$\mathbf{H}_k \approx \mathbf{H}_1 \mathbf{\Theta}_k, \tag{34}$$

for $k = 2, \ldots, Q-1$, where $\mathbf{\Theta}_k$ is a diagonal matrix denoting the evolution of the frequency response of the channel with respect to the first symbol. Note that Eq.(34) is an approximation which neglects the channel variation within the symbol duration. While frequency domain equalization aims at removing the effect of $\mathbf{H}_1$, $\mathbf{\Theta}_k$ can still impact the performance.

We propose here to use the sequence $\hat{\mathbf{s}}_{t,k}$ to update the estimate of the channel frequency response. Let us denote as $\mathbf{S}_t$ the $N_t \times N_t$ matrix having the frequency response of $\mathbf{s}_t$ in its diagonal, i.e. $\mathbf{S}_t = diag\,(\bar{\mathbf{s}}_t)$ where $\bar{\mathbf{s}}_t = \mathbf{F}_{N_t}\mathbf{s}_t$. An estimate of the evolution of the channel frequency response at symbol k can be then calculated as follows:

$$\hat{\boldsymbol{\theta}}_{\mathbf{k}} = \mathbf{S}_t^{-1}\hat{\mathbf{s}}_{t,k}. \tag{35}$$

In a practical implementation, advanced techniques such as Wiener filtering [27] can also be applied for improving the estimate of $\hat{\boldsymbol{\theta}}_{\mathbf{k}}$ rather than using the simple least square solution in Eq.(35). Note that a proper estimate of $\hat{\boldsymbol{\theta}}_{\mathbf{k}}$ assumes $\hat{\mathbf{s}}_{t,k}$ to experience a cyclic fading. Specific arrangements in the reference sequence design for enabling this will be discussed in the next subsection. The N_t-length vector $\hat{\boldsymbol{\theta}}_{\mathbf{k}}$ samples the channel frequency response with resolution equal to $(N/N_t)\,\Delta f$, and is then interpolated to a length N in order to obtain an estimate of $\boldsymbol{\Theta}_k$. MMSE equalization can be then run as in Eq.(33) by replacing $\hat{\mathbf{H}}_1$ with the updated channel estimate $\hat{\mathbf{H}}_k = \hat{\mathbf{H}}_1\hat{\boldsymbol{\Theta}}_k$. The data vector can be then retrieved as in Eq.(32).

The receiver here described is intended to be a baseline structure which paves the way for several optimizations. For instance, the current structure neglects the inter-carrier interference (ICI) arising at high Doppler and which can affect both channel estimate and symbol detection. Well-known ICI cancellation solutions, e.g., [36], [37], can be easily applied to this structure. Further, the estimation of the correction factor $\boldsymbol{\Theta}$ can be optimized by exploiting the statistical properties of the Doppler spread. This is left for future work.

A. REFERENCE SEQUENCE SELECTION AND MAPPING

We recommend here the usage of a cyclically extended ZC sequence $\mathbf{c}$ in the RS symbol of the UW DFT-s-OFDM frame. This allows to benefit from the ZC properties for the $\hat{\mathbf{H}}_1$ estimate. However, the sequence $\mathbf{s}_t$ which represent the tail of the IDFT of $\mathbf{c}$ and is used for estimating the correction factor $\boldsymbol{\Theta}_k$ does not enjoy the advantageous ZC properties. In particular, there is no guarantee of its flat frequency response. A frequency selective response of $\mathbf{s}_t$ may negatively affect the estimate of $\boldsymbol{\Theta}_k$ by enhancing the noise power over specific portions of the spectrum.

Nonetheless, the set of ZC sequences has a large cardinality and this offers the possibility to search for sequences having favorable tail properties. Given the sequence length N and being $\bar{N}$ the first prime number lower than N, $\bar{N}-1$ root ZC sequences exist. Further, for each root sequence, N different cyclic shifted version of the same sequence can be obtained, leading to a set of $N(\bar{N}-1)$ ZC sequences of length N. We can then search in this large set for sequences whose tail $\mathbf{s}_t$ enjoys a low frequency selective response. In particular, we propose to use a metric inspired to the known Wiener entropy [38] for assessing the frequency selectivity of $\bar{\mathbf{s}}_t$. Such metric reads

$$Z = \left| \frac{e^{\frac{1}{N_t}\sum_{n=0}^{N_t-1} ln(\bar{\mathbf{s}}_t[n])}}{\frac{1}{N_t}\sum_{n=0}^{N_t-1}\bar{\mathbf{s}}_t\,[n]} \right| - 1, \tag{36}$$

where $ln\,(\cdot)$ denotes the natural logarithm. In case $\bar{\mathbf{s}}_t$ is flat, Z=0. We can then search for sequences with $Z \approx 0$. In practice, the base station may store the indexes of a set of ZC sequences with very low Z metric. It can then assign them to users in critical Doppler conditions which are expected to exploit the tail of the signal for tracking the channel variations.

1) AVOIDING NON-CYCLIC ENERGY LEAKAGE

As mentioned in Section V, the estimate of $\boldsymbol{\Theta}_k$ suffers from the non-cyclic interference coming from the data part of the symbol. Such interference is due to the mismatch between the channel response estimated at the first symbol and used for equalization, and the instantaneous channel response. By following a principle similar to [39], we propose here to insert two tails at the end of the symbol in order to introduce a cyclic energy leakage on the second tail. The input vector in Eq.(1) reads then

$$\mathbf{q}_k = [\mathbf{s}_h \quad \mathbf{d}_k \quad \mathbf{s}_t \quad \mathbf{s}_t]^T, \tag{37}$$

where the data vector $\mathbf{d}_k$ now has length $N - N_h - 2N_t$. Obviously, this approach increases the overhead. However, it is intended to be applied to critical users such that the performance benefits obtained by improving the quality of the channel estimate compensate the penalty in terms of spectral efficiency. In the following, both options of single and double tails will be evaluated.

VI. NUMERICAL ANALYSIS

In this section, we evaluate numerically the performance of G-DFT-s-OFDM waveforms by Monte Carlo simulations. In particular, we address the signal properties, channel estimation reliability, and capability of tracking fast channel variations. We refer instead to [11] and [16] for a detailed link performance analysis.

A. SIGNAL PROPERTIES

An analysis of the characteristics of the transmit signals is carried out first. We assume here a configuration with N=1200, N_t=84, N_{IFFT}=2048, Δf=15 kHz, 16QAM modulation. When no differently specified, N_h is set to be 8 samples. The performance of OFDM and DFT-s-OFDM is also included for the sake of comparison. It is worth to mention that, with such settings, the corresponding N_{s_t}-long signal tail has the same duration as the CP of OFDM/DFT-s-OFDM in LTE (short CP configuration) [17].

Figure 10 shows the Complementary Cumulative Distribution Function (CCDF) of the PAPR of G-DFT-s-OFDM waveforms. It is well known from literature that DFT-s-OFDM exhibits lower PAPR than OFDM due to

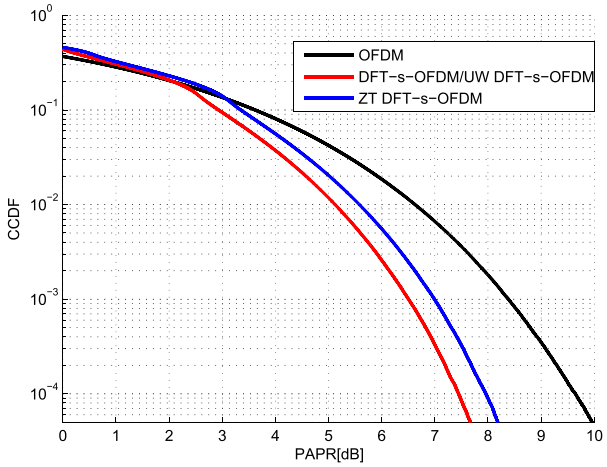

FIGURE 10. PAPR performance of G-DFT-s-OFDM, assuming 16QAM modulation.

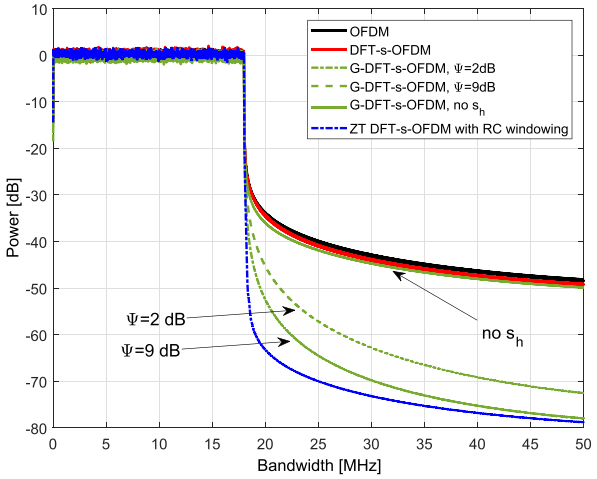

FIGURE 11. Ouf-of-band emissions of G-DFT-s-OFDM.

its *quasi*-single carrier nature [5]. This allows the transmit power amplifier to operate with a lower back-off, with remarkable advantages in terms of power efficiency. UW DFT-s-OFDM has obviously the same performance as DFT-s-OFDM. ZT DFT-s-OFDM introduces a PAPR penalty of around 0.5 dB due to the presence of the low power samples in the tail. However, a considerable performance margin over OFDM is preserved. Such PAPR penalty can in principle be avoided by transmitting only the samples in the interval $\left(N_{s_h} : N_{FFT} - N_{s_t} - 1\right)$, i.e. blanking with zeros the head and the tail of the signal; in this way, the power amplifier can be set to operate with the same back-off of DFT-s-OFDM. This option breaks the subcarrier orthogonality, however introducing a minor level of intercarrier interference given the low magnitude of the eliminated samples. It is worth to notice that the PAPR penalty of ZT DFT-s-OFDM is dependent on the effective overhead of N_{s_h} and N_{s_t}, which can be reduced in case of channels with low estimated delay spread.

Figure 11 displays the out-of-band emissions of G-DFT-s-OFDM, computed by using a Welch periodogram [31]. Different head sequence sizes, parametrized as a function of the Ψ parameter introduced in Section II.A, are considered. In case ZT DFT-s-OFDM and UW DFT-s-OFDM feature the same performance, an unique curve representative of G-DFT-s-OFDM is displayed. When the known $\mathbf{s}_h$ is not added, G-DFT-s-OFDM has approximately the same out-of-band emissions of OFDM/DFT-s-OFDM. However, the presence of both known $\mathbf{s}_h$ and $\mathbf{s}_t$ leads to significantly lower out-of-band emissions, thanks to the smooth transition between adjacent time symbols. The spectral power regrowth due to high Ψ values is rather limited; an extremely short head is sufficient for maintaining a low residual power on the adjacent bands. Note that, differently from known spectral shaping solutions such as raised cosine [40], the spectral containment of G-DFT-s-OFDM does not come at the expense of signal distortion, but it is a inner property of the waveform itself. The specific ZT DFT-s-OFDM case is particularly suited for the application of Raised Cosine (RC) windowing to further smoothen the symbol transitions and benefit in terms of spectral containment, as also shown in Figure 11. Since the windowing is applied over samples having already significant lower magnitude than the data samples, the distortion on the data part is expected to be minimal. A detailed analysis of the usage of raised cosine windowing with ZT DFT-s-OFDM is left for future work.

B. CHANNEL ESTIMATION PERFORMANCE

The challenges of mapping reference sequences and retrieving channel estimates in both ZT DFT-s-OFDM and UW DFT-s-OFDM have been extensively described in Section III. While the UW DFT-s-OFDM solution is rather straightforward, ZT DFT-s-OFDM requires a tailored channel estimator. We evaluate here the channel estimation performance of ZT DFT-s-OFDM assuming the estimator proposed in Section III.C, and also compare it with OFDM and UW DFT-s-OFDM. We consider the same configuration parameters as in Section VI.A, and N_{s_h}=8. The initial reference sequence $\mathbf{c}$ as a cyclically extended version of a ZC sequence having length L equal to the prime number 1109. Such sequence is then converted to time domain, eventually cyclic shifted and zero-padded according to Eq.(26) and Eq.(27), respectively, to fit the 1200 size. We consider the power delay profiles of Typical Urban [41] channel model, featuring an excess delay of around $\sim 2.2\mu s$, therefore significantly shorter than the low power tail duration. Performance is evaluated in terms of Mean Square Error (MSE) of the channel estimate in the frequency domain, which reads $MSE = E\left[\left|\mathbf{H} - \hat{\mathbf{H}}\right|^2\right]$, where $\mathbf{H}$ is the frequency response of the channel impulse response $\mathbf{h}$. The following three options are considered:

- **Option 1**. The traditional transmitter and channel estimator as in DFT-s-OFDM and UW DFT-s-OFDM are used. The estimation is then based on a RS with non-flat frequency response due to the zero-insertion (see Eq.(27)).

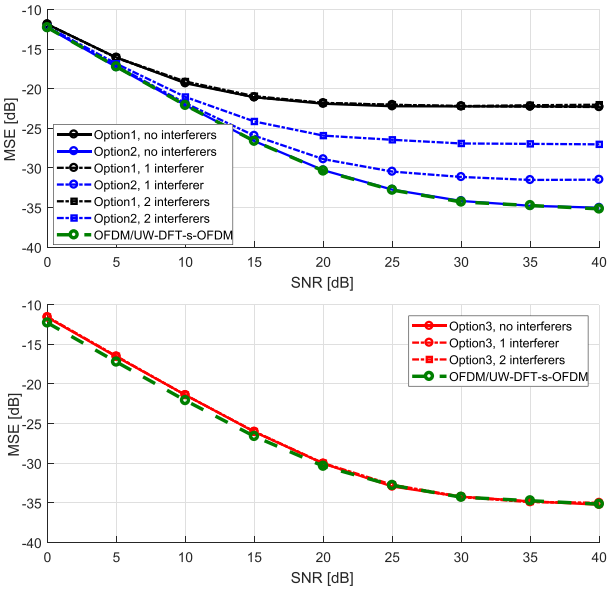

FIGURE 12. MSE of the channel estimate for ZT DFT-s-OFDM, assuming a Typical Urban channel.

- **Option 2**. The transmitter applies a deliberate distortion to the $\tilde{\mathbf{c}}_t^{\delta}$ sequence as described in [29] in order to force a flat frequency response $\tilde{\mathbf{c}}_f^{\delta}$. The estimator in Section III is used.
- **Option 3**. The traditional transmitter chain as in Section III is used, without signal distortion, and the new channel estimator described in Section IV.B is adopted.

Further, we consider the case when only the desired signal is transmitted, and the case with multiple users transmitting simultaneously by adopting a different cyclic shifted version of the same sequence. The cyclic shift is set to be significantly larger than the delay spread of the channel. Results are obtained upon transmission of 10000 ZT DFT-s-OFDM reference sequence symbols.

Figure 12 shows the MSE performance of the three options as a function of the Signal-to-Noise Ratio (SNR) for the Typical Urban channel. We have separated results from Option 1 and 2 from results of Option 3 for the sake of visual clarity. In noise-limited region, i.e. at low SNR, all the solutions perform similarly, while their behavior diverges at sufficiently high SNR. Option 1 suffers rather soon of a noise floor which is due to the poor autocorrelation property of the sequence $\tilde{\mathbf{c}}_t^{\delta}$. In case no interferers are present, Option 2 offers nearly the same MSE than Option 3 at the low-medium SNRs. A slight degradation can be noticed, due to the noise-coloring of the OLA process in Option 3; the performance gap is however negligible for practical purposes. When interferers are present, performance of Option 2 is however severely degraded, differently from Option 3. Option 2 is indeed penalized by the fact that different cyclic shifts of the same original sequence leads to different sequences with significant cross-correlation [29]. Note that, in Option 1, when interferers are present no further MSE increase is visible; poor autocorrelation has then a larger impact than interference on the quality of the channel estimate. Note that an unique curve is added for both CP-based waveforms and UW DFT-s-OFDM. The performance of these waveforms is indeed the same as Option 3 for ZT DFT-s-OFDM. This demonstrates the capability of the proposed estimator to overcome the drawbacks of the reference sequence mapping in ZT DFT-s-OFDM.

C. TRACKING FAST CHANNEL VARIATIONS

Differently from ZT DFT-s-OFDM, where the low power tail is only meant to absorb the delay spread of the radio channel and ensure smooth transition between adjacent symbols, in UW DFT-s-OFDM the known tail repeated at each symbol offers the possibility of updating the channel estimate besides coping with its cyclicity task. We evaluate here the potential of the channel tracking procedure presented in Section V. Let us consider a frame composed of 7 UW DFT-s-OFDM symbols, where the RS is allocated in the first symbol. Note that this corresponds to the interval between consecutive DMRS in LTE uplink [17]. The used configuration parameters are the same as Section VI.A and Section VI.B, with Δf=15 kHz. As mentioned above, the usage of $N_t = 84$ samples leads to a tail duration which corresponds to the CP duration in LTE. We consider the cases where a single tail (ST) and a double tail (DT) is used, according to Eq.(1) and Eq.(37); this leads to an overhead of 7.67% and 14.67%, respectively.

We evaluate performance in very harsh conditions: high speed up to 500 kmph and Typical Urban frequency selective channel profile. The time-varying profile of each channel tap is generated with the Clark/Gans model [42], assuming a carrier frequency of 2 GHz. Channel estimation and correction are based on a simple least square estimator. When no otherwise specified, we consider as RS a ZC sequence whose tail has a very low Z metric (below 0.01%).

Results are presented in terms of MSE of the channel estimate, and collected over 10000 frames transmission. In practice, $\mathbf{H}$ is calculated assuming the instantaneous power delay profile at the beginning of each symbol. For the channel estimation, no interpolation between the channel responses obtained across consecutive frames is considered. This may lead to rather pessimistic results. However, at very high speed such interpolation may even be detrimental due to the short coherence time. Further, interpolation across multiple frames forces the receiver to wait for the reception of the successive frame before detection can start, thus increasing the latency and disabling the possibility of exploiting efficient pipeline processing.

Figure 13 shows the MSE performance at different user speeds, considering two different SNR values. For the sake of comparison, we also include the options of no correction, as well as the result obtained with a RS with significantly high Z metric ($\approx$0.3). The no correction option refers to the case in which the channel estimated in the RS symbol is used for the MMSE equalization in all the data symbols, without exploiting the tail of the signal; this corresponds to the case

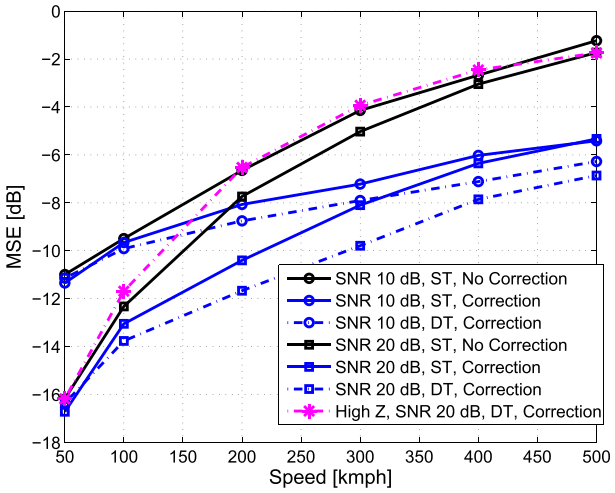

FIGURE 13. MSE of the channel estimate for UW DFT-s-OFDM.

of traditional DFT-s-OFDM, where the channel can only be estimated in DMRS symbols fully dedicated to that purpose. The gap between the no correction options at different SNRs is significant at low speed but tends to decrease at high speed, where the performance is dominated by the degradation of the channel estimate. The improvements obtained by processing the tail are negligible at low speed, but become significant as soon as the speed is higher than 100 kmph. The usage of a double tail (DT configuration) leads to a further reduction of the MSE. Such reduction is more evident at high SNR, where the benefits introduced by cyclicity dominate over the residual noise. As expected, the usage of a sequence with high Z metric leads to even worse performance than no correction, since the frequency selective profile of the tail leads to a wrong correction factor.

VII. CONCLUSIONS AND FUTURE WORK

In this article, we have described the properties of Generalized DFT-s-OFDM (G-DFT-s-OFDM) waveforms without CP, with the particular emphasis on challenges and opportunities related to channel estimation and tracking. Both Zero Tail (ZT) DFT-s-OFDM and Unique Word (UW) DFT-s-OFDM solutions are presented and analyzed. G-DFT-s-OFDM replace the CP with an internal guard interval whose length can be set dynamically according to the delay spread of the channel rather than being hardcoded in the system numerology. This eases scalability as well as coexistence among cells operating over channels with diverse dispersion characteristics. Such waveforms are particularly suited for TDD mode given the opportunity of embedding the guard period in the symbol itself, as well as for fast beam switching at mm-wave frequencies. G-DFT-s-OFDM also features attractive properties in terms of PAPR and spectral containment even without additional filtering/windowing, thus supporting asynchronous access and coexistence of flexible numerologies in the same carrier. Channel estimation requires specific arrangements either on the frame design (for UW DFT-s-OFDM) or at the receiver processing (for ZT DFT-s-OFDM) in order to fully exploit the nominal properties of the used reference sequences. The usage of the same signal tail at each symbol also allows to track fast channel variations even without additional overhead.

Future work will address the performance of such waveforms with additional windowing and filtering operations, especially for the case of ZT DFT-s-OFDM whose low power head and tail makes it particularly suited for tolerating edge distortions. Future analysis will also focus to detailed performance assessment of G-DFT-s-OFDM for small bandwidth allocations, which may suffer from non-negligible energy leakage in the signal tail. The usage of ICI cancellation receivers and enhanced channel estimators is also to be considered for the sake of improving the capability of tracking fast channel variations.

REFERENCES

[1] L. Hanzo, M. Münster, B. Choi, and T. Keller, *OFDM and MC-CDMA for Broadband Multi-User Communications, WLANs and Broadcasting*. Hoboken, NJ, USA: Wiley, 2003.
[2] H. Holma and A. Toskala, Eds., *LTE Advanced: 3GPP Solution for IMT-Advanced*. Hoboken, NJ, USA: Wiley, 2012.
[3] P. Roshan and J. Leary, *802.11 Wireless LAN Fundamentals*. Indianapolis, IN, USA: Cisco Press, 2004.
[4] *Study on Scenarios and Requirements for Next Generation Access Technologies*, document 38.913, 3rd Generation Partnership Project, 2016.
[5] H. G. Myung, J. Lim, and D. J. Goodman, "Single carrier FDMA for uplink wireless transmission," *IEEE Veh. Technol. Mag.*, vol. 1, no. 3, pp. 30–38, Sep. 2006.
[6] F. Schaich and T. Wild, "Subcarrier spacing—A neglected degree of freedom?" in *Proc. IEEE 16th Int. Workshop Signal Process. Adv. Wireless Commun. (SPAWC)*, Jun./Jul. 2015, pp. 56–60.
[7] G. Wunder *et al.*, "5GNOW: Non-orthogonal, asynchronous waveforms for future mobile applications," *IEEE Commun. Mag.*, vol. 52, no. 2, pp. 97–105, Feb. 2014.
[8] G. Berardinelli, K. Pedersen, T. B. Sørensen, and P. Mogensen, "Generalized DFT-spread-OFDM as 5G waveform," *IEEE Commun. Mag.*, vol. 54, no. 11, pp. 99–105, Nov. 2016.
[9] B. Farhang-Boroujeny, "OFDM versus filter bank multicarrier," *IEEE Signal Process. Mag.*, vol. 28, no. 3, pp. 92–112, May 2011.
[10] N. Michailow *et al.*, "Generalized frequency division multiplexing for 5th generation cellular networks," *IEEE Trans. Commun.*, vol. 62, no. 9, pp. 3045–3061, Sep. 2014.
[11] G. Berardinelli, F. M. L. Tavares, T. B. Sørensen, P. Mogensen, and K. Pajukoski, "Zero-tail DFT-spread-OFDM signals," in *Proc. IEEE Globecom Workshops*, Dec. 2013, pp. 229–234.
[12] A. Sahin, R. Yang, M. Ghosh, and R. L. Olesen, "An improved unique word DFT-spread OFDM scheme for 5G systems," in *Proc. IEEE Globecom Workshops*, Dec. 2015, pp. 1–6.
[13] U. Kumar, C. Ibars, A. Bhorkar, and H. Jung, "A waveform for 5G: Guard interval DFT-s-OFDM," in *Proc. IEEE Globecom Workshops*, Dec. 2015, pp. 1–6.
[14] B. M. Popovic, "Generalized chirp-like polyphase sequences with optimum correlation properties," *IEEE Trans. Inf. Theory*, vol. 38, no. 4, pp. 1406–1409, Jul. 1992.
[15] G. H. Myung and J. D. Goodman, *Single Carrier FDMA: A New Air Interface for Long Term Evolution*. Hoboken, NJ, USA: Wiley, 2008.
[16] G. Berardinelli, F. M. L. Tavares, T. B. Sørensen, P. Mogensen, and K. Pajukoski, "On the potential of zero-tail DFT-spread-OFDM in 5G networks," in *Proc. IEEE 80th Veh. Technol. Conf. (VTC-Fall)*, Sep. 2014, pp. 1–6.
[17] H. Holma and A. Toskala, Eds., *LTE for UMTS: OFDMA and SC-FDMA Based Radio Access*. Hoboken, NJ, USA: Wiley, 2009.
[18] L. A. M. R. de Temino, G. Berardinelli, S. Frattasi, and P. Mogensen, "Channel-aware scheduling algorithms for SC-FDMA in LTE uplink," in *Proc. IEEE 19th Int. Symp. Pers., Indoor Mobile Radio Commun. (PIMRC)*, Sep. 2008, pp. 1–6.

[19] G. Berardinelli, K. Pajukoski, E. Lahetkangas, R. Wichman, O. Tirkkonen, and P. Mogensen, "On the potential of OFDM enhancements as 5G waveforms," in *Proc. IEEE 79th Veh. Technol. Conf. (VTC-Spring)*, May 2014, pp. 1–5.

[20] M. Lampinen, F. Del Carpio, T. Kuosmanen, T. Koivisto, and M. Enescu, "System-level modeling and evaluation of interference suppression receivers in LTE system," in *Proc. IEEE 75th Veh. Technol. Conf. (VTC-Spring)*, May 2012, pp. 1–5.

[21] S. Haykin, M. Sellathurai, Y. D. Jong, and T. Willink, "Turbo-MIMO for wireless communications," *IEEE Commun. Mag.*, vol. 42, no. 10, pp. 48–53, Oct. 2004.

[22] D. Catania, M. G. Sarret, A. F. Cattoni, F. Frederiksen, G. Berardinelli, and P. Mogensen, "The potential of flexible UL/DL slot assignment in 5G systems," in *Proc. IEEE 80th Veh. Technol. Conf. (VTC-Fall)*, Sep. 2014, pp. 1–6.

[23] P. Mogensen *et al.*, "B4G local area: High level requirements and system design," in *Proc. IEEE Globecom Workshops*, Dec. 2012, pp. 613–617.

[24] *LTE Physical Layer—General Description (Release 8)*, document TS 36201, V8.1.0, 3rd Generation Partnership Project, Nov. 2007.

[25] E. Lähetkangas *et al.*, "On the selection of guard period and cyclic prefix for beyond 4G TDD radio access network," in *Proc. Eur. Wireless Conf. (EW)*, Apr. 2013, pp. 1–5.

[26] A. Ghosh *et al.*, "Millimeter-wave enhanced local area systems: A high-data-rate approach for future wireless networks," *IEEE J. Sel. Areas Commun.*, vol. 32, no. 6, pp. 1152–1163, Jun. 2014.

[27] Y. Li, "Pilot-symbol-aided channel estimation for OFDM in wireless systems," *IEEE Trans. Veh. Technol.*, vol. 49, no. 4, pp. 1207–1215, Jul. 2000.

[28] *Uplink Reference Signal in EUTRA*, document R1-062642, 3GPP TSG-RAN WG1 Meeting 46bis, Oct. 2006.

[29] G. Berardinelli, F. Frederiksen, K. Pedersen, P. Mogensen, and K. Pajukoski, "Reference sequence design for zero-tail DFT-spread-OFDM," in *Proc. IEEE Wireless Commun. Netw. Conf. (WCNC)*, Apr. 2016, pp. 1–6.

[30] G. Berardinelli, K. I. Pedersen, F. Frederiksen, P. Mogensen, and K. Pajukoski, "A novel channel estimator for zero-tail DFT-spread-OFDM," in *Proc. Int. Symp. Wireless Commun. Syst. (ISWCS)*, Sep. 2016, pp. 373–377.

[31] S. Salivahanan and A. Vallavaraj, *Digital Signal Processing*. New York, NY, USA: McGraw-Hill, 2001.

[32] P. D. Papadimitriou and C. N. Georghiades, "Zero-padded OFDM with improved performance over multipath channels," in *Proc. 1st IEEE Consum. Commun. Netw. Conf. (CCNC)*, Jan. 2004, pp. 31–34.

[33] B. Muquet, Z. Wang, G. B. Giannakis, M. D. Courville, and P. Duhamel, "Cyclic prefixing or zero padding for wireless multicarrier transmissions?" *IEEE Trans. Commun.*, vol. 50, no. 12, pp. 2136–2148, Dec. 2002.

[34] G. Berardinelli, K. Pedersen, F. Frederiksen, T. B. Sørensen, and P. Mogensen, "Unique Word DFT-spread-OFDM for fast time varying channels," in *Proc. 85th IEEE Veh. Technol. Conf. (VTC-Spring)*, Jun. 2017, pp. 1–6.

[35] B. E. Priyanto, H. Codina, S. Rene, T. B. Sørensen, and P. Mogensen, "Initial performance evaluation of DFT-spread OFDM based SC-FDMA for UTRA LTE uplink," in *Proc. IEEE 65th Veh. Technol. Conf. (VTC-Spring)*, Apr. 2007, pp. 3175–3179.

[36] A. Seyedi and G. J. Saulnier, "General ICI self-cancellation scheme for OFDM systems," *IEEE Trans. Veh. Technol.*, vol. 54, no. 1, pp. 198–210, Jan. 2005.

[37] Y. Mostofi and D. C. Cox, "ICI mitigation for pilot-aided OFDM mobile systems," *IEEE Trans. Wireless Commun.*, vol. 4, no. 2, pp. 765–774, Mar. 2005.

[38] J. D. Johnston, "Transform coding of audio signals using perceptual noise criteria," *IEEE J. Sel. Areas Commun.*, vol. SAC-6, no. 2, pp. 314–332, Feb. 1988.

[39] J. Kim, S. Lee, and J. Seo, "Synchronization and channel estimation in cyclic postfix based OFDM system," in *Proc. IEEE 63rd Veh. Technol. Conf. (VTC-Spring)*, May 2006, pp. 2028–2032.

[40] J. Proakis, *Digital Communications*, 4th ed. New York, NY, USA: McGraw-Hill, 2001.

[41] *Deployment Aspects*, document TR 25.943, V6.0.0, 3rd Generation Partnership Project, 2005.

[42] M. Mfeze and E. Tonye, "Comparative approach of Doppler spectra for fading channel modelling by the filtered white Gaussian noise method," *Int. J. Comput. Sci. Telecommun.*, vol. 6, no. 11, pp. 1–12, Dec. 2015.

GILBERTO BERARDINELLI received the bachelor's and master's degrees (*cum laude*) in telecommunication engineering from the University of L'Aquila, Italy, in 2003 and 2005, respectively, and the Ph.D. degree from Aalborg University, Denmark, in 2010. He is currently an Associate Professor at the Wireless Communication Networks Section, Aalborg University, also in tight cooperation with Nokia Bell Laboratories. His research interests are mostly focused on physical layer, medium access control, and radio resource management design for 5G systems.